

4D Generic Video Object Proposals

Aljoša Ošep, Paul Voigtlaender, Mark Weber, Jonathon Luiten, and Bastian Leibe
 Computer Vision Group
 Visual Computing Institute
 RWTH Aachen University, Germany

{osep, voigtlaender, luiten, leibe}@vision.rwth-aachen.de mark.weber1@rwth-aachen.de

Abstract

Many high-level video understanding methods require input in the form of object proposals. Currently, such proposals are predominantly generated with the help of networks that were trained for detecting and segmenting a set of known object classes, which limits their applicability to cases where all objects of interest are represented in the training set. This is a restriction for automotive scenarios, where unknown objects can frequently occur. We propose an approach that can reliably extract spatio-temporal object proposals for both known and unknown object categories from stereo video. Our 4D Generic Video Tubes (4D-GVT) method leverages motion cues, stereo data, and object instance segmentation to compute a compact set of video-object proposals that precisely localizes object candidates and their contours in 3D space and time. We show that given only a small amount of labeled data, our 4D-GVT proposal generator generalizes well to real-world scenarios, in which unknown categories appear. It outperforms other approaches that try to detect as many objects as possible by increasing the number of classes in the training set to several thousand.

1. Introduction

The main result of this paper is a novel approach for generating high-quality spatio-temporal object tube proposals for both *known* and *unknown* objects from stereo video. The resulting tube proposals are localized in 3D space and capture the evolution of an object’s visible area over time, *i.e.*, they provide a temporally consistent object segmentation over a video sequence. Such tube proposals can be useful as basic primitives for a wide variety of applications, ranging from object tracking [58, 27, 36, 38, 22], to action/activity recognition [16], object category discovery [43, 22, 55, 59, 46, 24, 23, 48, 50, 65, 56], and zero-shot learning [62, 44, 1]. In particular, they are of great importance for automotive applications, in which the capability to perceive and react to unseen-before dynamic objects is a vital safety concern (see Fig. 1).



Figure 1: We propose a method for generating 4D video-object tube proposals of arbitrary objects from real-world videos and demonstrate generalization to objects of unknown categories. We evaluate our method on the Oxford RobotCar dataset, captured from a car [30].

Up to now, high-quality object tube proposals could only be generated either by (1) applying a pre-trained object detector for known classes and performing instance segmentation in every frame [11]; or by (2) starting from a manual object mask initialization and applying a video object segmentation approach [29, 57, 18, 3]. The significant contribution of our approach is that it can provide a compact set of high-quality object tubes with automatic initialization, while scaling well to novel, unseen-before object classes.

This result opens up exciting possibilities for many applications that can take tube proposals as their input. In particular, our approach is efficient enough that it can be applied for video mining in large video collections. We demonstrate its capabilities by applying it for object tube mining on 14h of driving video (8 million frames) of the Oxford RobotCar dataset [30]. We compare the obtained results to the Mask^X R-CNN approach by [17] (which tries to detect as many objects as possible by increasing the number of classes in the training set to 3,000). Our results show that

our approach (4D-GVT) achieves a similar level of recall for known and a higher recall for unknown objects, despite only using knowledge about the 80 COCO classes. In addition, our approach provides additional object information (trajectory, temporal extent, 3D size) that can be directly used for spatio-temporal object localization.

The key idea behind our approach is to make use of parallax as a cue to identify temporally consistent object tubes under egomotion of the recording vehicle. We leverage recent developments in object instance segmentation [11] and make use of stereo and sparse scene flow cues, which are readily available in an automotive scenario, to enforce consistency checks on possible tube continuations. In a nutshell, our proposed 4D-GVT method extends Mask R-CNN [11] to extract frame-level object proposals and their segmentation masks for arbitrary objects. It then localizes these image regions in 3D space and predicts their 3D motion. Taking parallax as a consistency filter, our approach narrows down the potentially huge set of tube continuations to those that are consistent with the object’s perceived relative motion. As a result, 4D-GVT is able to quickly trim down a large initial set of frame-level region proposals and turn them into a temporally consistent set of object tubes with accurately tracked object positions. In fact, our experiments show that when applying our 4D-GVT proposal generator for car and pedestrian tracking on the KITTI dataset [7], it reaches close to state-of-the-art performance even when compared to dedicated tracking-by-detection methods.

We believe that our proposed 4D-GVT approach is a promising contribution for generating generic 4D proposals belonging to both known and unknown categories. In particular, we expect that it has a great potential to provide the basic primitives that future action recognition, object discovery, or zero-shot learning approaches can be built upon. We will make all code and data available upon publication.

1.1. Related Work

Video-Object Mining. Video-Object mining (VOM) refers to a task of pattern discovery in video collections. It has been used for improving object detectors by mining hard-negatives for specific object categories from web-videos [51, 20], for learning new detectors for objects by localizing mostly single, dominant objects in videos and for tracking-based semi-supervised learning, in which sparse annotations extended by tracks were leveraged in order to extend the amount of training data [31, 32]. The task is not limited to image-video data, but Teichman *et al.* [53] propose a method for tracking-based semi-supervised learning by mining LiDAR streams, captured from a vehicle.

Multi-Object Tracking. The above-mentioned methods have in common that they all require object tracking capabilities. (Multi)-Object tracking is a field with a long research history, originating from a range of sensory modal-

ties, such as RADAR [45]. The dominant approach for vision-based multi-object tracking is tracking-by-detection. For that, detection signals of potential objects originate from images and are usually extracted from image data by a pre-trained object detector [25, 63]. The drawback of such methods is that they can only track objects, for which a sufficient amount of training data is available. In realistic scenarios, however, it is not feasible to obtain training data for every possible object of interest. For that reason, the most common approach in the robotics community to object tracking is based on unsupervised segmentation of 3D sensory data using information such as spatial proximity and motion cues and tracking objects in a category-agnostic setting [5, 13, 14, 53, 52, 34]. There are a few methods that proposed similar ideas in the vision community by using image-based object proposals as leads for tracking [64, 58, 27, 22, 15], often leveraging stereo information [36, 38, 33, 26] or motion cues [54] as an additional lead for obtaining object proposals.

Video-Object Segmentation. Alternatively, object instances can be mined from video using video-object segmentation (VOS), which refers to a task of segmenting objects in videos with weak supervision [57, 18, 3]. Existing methods, however, require either supervision for the first video frame in the form of pixel masks or are limited to moving objects in an unsupervised setting [58, 27]. Rünz *et al.* [47] propose another closely related method for moving object tracking, segmentation and integration within a dynamic SLAM framework using RGBD sensors. Different from our approach, their method is limited to a set of a-priori *known* classes. Our proposed 4D-GVT method leverages well-understood concepts from classic tracking methods [45, 25] and, similar to video-object segmentation methods in the unsupervised setting, segments objects at the pixel level in the videos to obtain video tubes for both moving and stationary objects. Furthermore, the proposed method extends the localization of objects to 3D space.

Open-set Segmentation. Many real-world scenarios require reliable segmentation that is not limited to a few categories for which fully labelled training data is available. Mask^X R-CNN [17] tackles this problem by using partial supervision of bounding boxes to perform instance segmentation for the Visual Genome dataset that includes 3000 categories. Pham *et al.* [40] address the problem of open-set segmentation by fusing modern instance segmentation with traditional unsupervised methods to obtain instance segmentation for an unbounded number of categories. In contrast, our model leverages its in-built category-agnostic detection to generalize to objects of *unknown* categories on a video-level without requiring additional supervision.

Possible Applications. Our 4D-GVTs are a flexible tool that can be used for many different applications. A particularly interesting application for object proposals is the au-

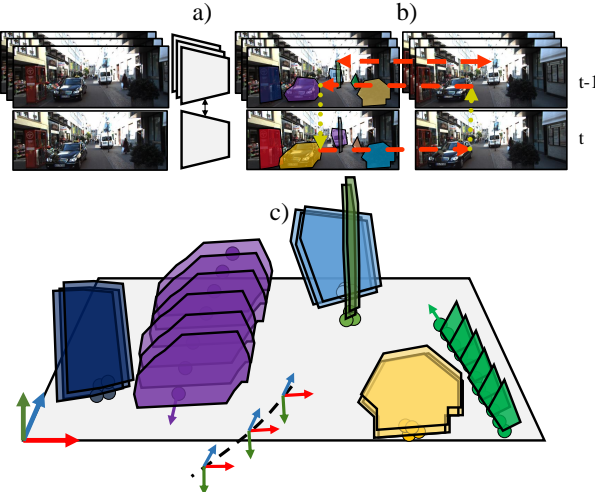


Figure 2: We obtain 4D Video Tubes by a) extracting frame-level object proposals from a video stream using a pre-trained network, b) match features in order to estimate depth and sparse scene flow to localize proposals in 3D and estimate their velocity and finally, c) associate these 3D segments to obtain a set of video tubes.

tomatic discovery of new object categories [46, 24, 23, 48, 50, 65, 56], a task related to zero-shot learning [62, 44, 1]. Video-based object discovery has so far been addressed using weak [59], semantic [55] or no supervision [43, 22]. However, most current methods are limited to only simple scenarios containing a single or only a few objects of interest. In contrast, our approach addresses real-world scenarios, captured from mobile platforms, in which several objects per image typically occur.

2. Method

We first provide a brief outline of our approach and then introduce its steps in detail. We mine a compact set of 4D Video Tubes as follows. From each video-frame of the video sequence, we obtain a set of ranked image-level object proposals (Fig. 2, a), defined by an object pixel mask. Next, we localize these mask proposals in 3D space (camera coordinate frame) using the stereo-based depth estimator from [8] and predict their motion by computing sparse scene flow, obtained by matching image features (Fig. 2, b). Using the estimated depth and pixel mask, we localize 3D segments of these proposals in 3D space and associate them in space-time in order to obtain a set of 4D Video Proposal Tubes (Fig. 2, c). To obtain a compact set of tubes we score them using 1) objectness, 2) motion and 3) temporal mask consistency cues and perform an additional optimization step that suppresses tubes with significant overlap in space-time. In the following, we provide a detailed outline of each step of our method.

2.1. Image-Level Proposals with MP R-CNN

First, we need to obtain cues for potential objects on the video-frame level. One option would be to obtain instances of *known* object categories for each video frame using Mask R-CNN [11]. The Mask R-CNN detector is excellent at identifying objects that appear during training. However, we do not want to limit ourselves to obtaining image-level cues only for the most common object categories for which we can obtain a sufficient amount of training data.

For this purpose, we propose a category-agnostic extension of Mask R-CNN, Mask Proposal R-CNN (MP R-CNN), whose classification part only disambiguates objects from the background. We achieve that by first training the network in the category-agnostic setting, *i.e.* by merging all 80 COCO classes into one “object” class. By only distinguishing between objects and non-objects (according to the COCO category definitions), we expect a better generalization to object categories that are either not present or not annotated in COCO. We confirm experimentally in Sec. 3 that this procedure indeed generalizes to unseen object classes (*i.e.*, classes not present in COCO). In order to retain a capability to perform higher-granularity classification for objects that appeared in the training set, we add a second classification head (identical to the normal classification head of Mask R-CNN) to this network which disambiguates between the 80 classes. At test time, the category-agnostic classification head is used to provide confidence scores for proposals, and the second classification head is additionally evaluated to provide a posterior distribution over the 80 classes for each proposal.

By thresholding the confidence of the class-specific classification head, we can again divide the proposals into a class-specific and a class-agnostic set. By adding the category-specific head, we thus retain class information when it is available and achieve a performance comparable to the class-specific version, while still retaining a good generalization ability to unseen classes due to the category-specific head as our experiments demonstrate.

2.2. 4D Video Tubes

To get from image-level proposals to 4D Video Tubes, we combine modern instance segmentation methods (trained on large-scale datasets [28]) with standard object tracking methods [25, 45]. Formally, we obtain a set of frame-level object proposals $\mathcal{P}^{0:T}$ in the frame-range $0 \rightarrow T$, $\mathcal{P}^t = \{\mathcal{S}_j^t, t \in 0 \dots T\}$ from MP R-CNN. The j -th per-frame proposal is defined as $\mathcal{S}_j^t = [\mathbf{p}_j^t, \mathbf{v}_j^t, \mathbf{s}_j^t, \mathbf{c}_j^t, \mathbf{m}_j^t, \mathbf{s}^t]$. The mask $\mathbf{m} \in \{0, 1\}^{w \times h}$ for an image of size $w \times h$, objectness score $\mathbf{s} \in [0, 1]$ and category information $\mathbf{c} \in \mathbb{R}^{81}$ (*i.e.* one of *known* 80 COCO classes or *unknown*) are obtained by the MP R-CNN network. This information is extended by 3D position $\mathbf{p} \in \mathbb{R}^3$, 3D size $\mathbf{s} \in \mathbb{R}^3$ and velocity

vector $\mathbf{v} \in \mathbb{R}^3$ from the video sequence as follows. For each video sequence, we match local Harris corner based image features of 1) left-right images coming from stereo and 2) forward-backward in time for two consecutive neighboring frames $(t-1) \rightarrow t$. Features that pass a cyclic consistency check (left, right, forward, backward) are used to estimate sparse scene flow. We triangulate left-right matches in two consecutive frames and compute difference vectors $((t-1) \rightarrow t)$ for all successful matches.

Using the same set of feature matches, we obtain an egomotion estimate $E^{(t-1) \rightarrow t}$ by minimizing the re-projection error using a non-linear least squares method [9] and finally keeping left-right image matches to obtain a scene depth estimate D^t using the feature-matching based method of [8]. This technique reduces the set of proposals in case of depth estimation failure, typically only occurring for objects at a far distance. Next, we subtract the estimated egomotion vector from the sparse-flow estimates in order to obtain a sparse set of velocity estimates. The velocity of the frame-level object proposal is computed by averaging the inner-quartile of velocity estimates within the image area of the estimated mask. The 3D position of the proposal is estimated as the median of the 3D points coming from the depth map and lying within the mask area. Similarly, the objects 3D size is estimated by fitting a 3D bounding box based on the inner-quartile of 3D points surrounding the estimated median 3D position.

Video Tube Proposals After obtaining a set of per-frame object proposals $\mathcal{P}^{0:T}$ for a video sequence that spans from frame $0 \rightarrow T$, we need to partition these into a 4D tube proposal set, *i.e.*, a set of video tube proposals $\mathcal{A}^{0:T} = \{\mathcal{T}_i^{n:m}\}$, where each tube proposal \mathcal{T}_i spans over a frame range of n to m . In the following, we do not differentiate between *known* and *unknown* proposals.

Obtaining such partitions is a very challenging, multi-dimensional assignment problem: Object proposals may originate from tracked objects and segmentation clutter. Different to standard tracking-by-detection based methods, where object detectors narrow down proposals to typically 1 – 20, we obtain roughly 300 – 400 possibly relevant object proposals per frame. Obtaining an exact solution to multi-frame assignment problems in tracking is NP-hard, and we need to resort to approximate solutions. One possibility would be to use an approach like MHT [45], which maintains a tree of potential associations for each possible object and to perform tree pruning in order to avoid combinatorial explosion. However, for a large number of per-frame object proposals, maintaining such a tree would be prohibitively expensive.

Instead, we resort to the forward-backward track enumeration algorithm [25]. We perform a forward-backward data association by sliding a temporal window over the whole video sequence. For each video frame t , $t \in 0 \dots T$,

we 1) extend the existing tube proposal set using \mathcal{P}^t and 2) attempt to start a new object tube from each unassigned 3D proposal by performing reverse-time data association within a temporal window. As soon as no association can be performed for a number of frames, the tube proposal is terminated. Indeed this means that we may have split a real-world object tube into several sub-tubes, but we consider that a reasonable trade-off.

In order to minimize incorrect associations, which would lead to spurious tubes, we leverage object motion models, the rigidity of the 3D scene, and the known image formation model to guide frame-to-frame proposal data association to only a small set of feasible associations. This is done as follows (similar to [38]). Using an estimate of frame-level object proposals with 3D position \mathbf{p} , velocity \mathbf{v} and size \mathbf{s} from each frame-level proposal, we start a new tube proposal and estimate its state recursively using a linear Kalman filter. In particular, we keep track of the object’s 3D position, velocity, and 3D size. We perform association in the following steps. First, we perform a Kalman filter prediction in order to estimate a 3D position and perform 3D position based gating in order to severely narrow down the set of feasible proposal associations. Then, we predict the segmentation mask of the object in the current frame, and finally we extend the tube with the proposal that maximizes joint association probability based on mask IoU (image domain) and 3D position.

We obtain the mask prediction $\mathbf{m}_i^{(t-1) \rightarrow t} \in \{0, 1\}^{w \times h}$ of tube \mathcal{T}_i for video-frame $t \in 1 \dots T$ based on a 2D mask estimate of the last associated mask $\mathbf{m}_i^{(t-1)}$, the depth prediction D^t and the egomotion estimate $E^{(t-1) \rightarrow t}$:

$$\begin{aligned} \mathcal{J} &= \pi(K E^{(t-1) \rightarrow t} M_i^{(t-1) \rightarrow t} K^{-1} \pi^{-1}(\mathbf{m}_i^{(t-1)} \odot D^{(t-1)})), \\ \mathbf{m}_i^{(t-1) \rightarrow t}(\mathbf{p}') &= \begin{cases} 1, \mathbf{p}' \in \mathcal{J} \\ 0, \text{else} \end{cases}, \end{aligned} \quad (1)$$

where $\pi : \mathbb{R}^3 \rightarrow \mathbb{R}^2$ and $\pi^{-1} : \mathbb{R}^2 \rightarrow \mathbb{R}^3$ denotes camera projection/backprojection operator (applied element-wise), K denotes a known camera matrix and \odot performs element-wise multiplication. The matrix $M_i^{(t-1) \rightarrow t}$ represents estimated motion of the tube by the Kalman filter.

Thus, starting from the per-frame proposals $\mathcal{P}^{0:T}$ over the video sequence, obtained from the MP R-CNN network and localized in 3D space, we have now linked these proposal segments together into a set of proposal video tubes $\mathcal{A}^{0:T}$. These proposal tubes may still overlap with each other and provide competing explanations for the same image pixels. We therefore need to score them in order to make a selection for a consistent scene interpretation.

Scoring Tube Proposals. We obtain a ranked set of relevant video tube proposals by scoring tubes using log-likelihood ratios [45] between the proposal tube and the null tube (null track hypothesis in MHT [45] terminology). The null tube encodes tubes generated from random background

clutter. The score $\theta(\cdot)$ of the tube \mathcal{T}_i is a linear combination of the tube motion score, the mask consistency score and the tube objectness score (we are omitting time indices for brevity):

$$\theta(\mathcal{T}_i) = w_1 \cdot \vartheta_{\text{motion}}(\mathcal{T}_i) + w_2 \cdot \vartheta_{\text{mask}}(\mathcal{T}_i) + w_3 \cdot \vartheta_{\text{obj}}(\mathcal{T}_i). \quad (2)$$

Intuitively, the tube motion score encodes the assumption that objects move smoothly. It takes the form of a likelihood ratio test, comparing the probability that the tube corresponds to a valid object tube to the null hypothesis that the tube was generated from random background clutter:

$$\vartheta_{\text{motion}}(\mathcal{T}_i^{n:m}) = \ln \frac{p(\mathbf{p}_{\mathcal{T}_i}^{n:m} | \mathcal{I}_i \subseteq \mathcal{T}_i^{n:m})}{p(\mathbf{p}_{\mathcal{T}_i}^{n:m} | \mathcal{I}_i \subseteq \mathcal{T}_\emptyset)}, \quad (3)$$

the notation $\mathcal{I}_i \subseteq \mathcal{T}_i^{n:m}$ denotes that the 3D position observations originate from the tube $\mathcal{T}_i^{n:m}$ and \mathcal{T}_\emptyset denotes the null tube hypothesis. The set $\mathcal{T}_i^{n:m} = \{\mathcal{S}_{k_i}^t \mid n \leq t \leq m\}$ denotes the supporting image-level proposal set of a tube, where k_i refers to the k -th frame-level proposal that supports \mathcal{T}_i at a certain frame t . The Markovian motion assumption and conditional independence assumption of the observations originating from the null tube hypothesis lead to the following factorization of Eq. 3:

$$\begin{aligned} p(\mathbf{p}_{\mathcal{T}_i}^{n:m} | \mathcal{I}_i \subseteq \mathcal{T}_i^{n:m}) &= \prod_{t=n}^m p(\mathbf{p}^t | \mathbf{p}_{\mathcal{T}_i}^{(n-1):(t-1)}, \mathcal{I}_i \subseteq \mathcal{T}_i^{n:t}) \\ &= \prod_{t=n}^m \mathcal{N}(\mathbf{p}^t; \mathbf{p}_{\text{pred}}^{(t-1) \rightarrow t}, \Sigma_{\text{pred}}^{(t-1) \rightarrow t}), \end{aligned} \quad (4)$$

$$p(\mathbf{p}_{\mathcal{T}_i}^{n:m} | \mathcal{I}_i \subseteq \mathcal{T}_\emptyset) = \prod_{t=n}^m p(\mathbf{p}_{\mathcal{T}_i}^t | \mathcal{I}_i \subseteq \mathcal{T}_i) = \prod_{t=n}^m \frac{1}{A_{\text{GP}}}. \quad (5)$$

The likelihood that the observation originates from the tube is assumed to be Gaussian [45] and is evaluated using the Kalman filter prediction. It measures how well the ground position of an object proposal corresponds to the Kalman filter prediction $\mathbf{p}_{\text{pred}}^{(t-1) \rightarrow t}$ under the estimated variance $\Sigma_{\text{pred}}^{(t-1) \rightarrow t}$ at time t . This is evaluated against the null hypothesis of a uniform distribution of clutter objects over the sensing area A_{GP} (roughly $80m \times 50m$ of the ground plane, estimated from the 3D point cloud).

The tube mask consistency score encodes the intuition that the silhouette and position of the object in the image plane do not change significantly on a frame-to-frame level. Again, a likelihood ratio test is used, comparing the mask IoU against a null hypothesis model of no intersection:

$$\vartheta_{\text{mask}}(\mathcal{T}_i^{n:m}) = \ln \frac{p(\mathbf{m}_{\mathcal{T}_i}^{n:m} | \mathcal{I}_i \subseteq \mathcal{T}_i^{n:m})}{p(\mathbf{m}_{\mathcal{T}_i}^{n:m} | \mathcal{I}_i \subseteq \mathcal{T}_\emptyset)}, \quad (6)$$

following the same assumption as for (3), (6) factorizes as:

$$\begin{aligned} p(\mathbf{m}_{\mathcal{T}_i}^{n:m} | \mathcal{I}_i \subseteq \mathcal{T}_i^{n:m}) &= \prod_{t=n}^m p(\mathbf{m}^t | \mathbf{m}_{\mathcal{T}_i}^{(n-1):(t-1)}, \mathcal{I}_i \subseteq \mathcal{T}_i^{n:t}) \\ &= \prod_{t=n}^m \text{IoU}(\mathbf{m}^{(t-1) \rightarrow t}, \mathbf{m}^t) \end{aligned} \quad (7)$$

$$p(\mathbf{m}_{\mathcal{T}_i}^{n:m} | \mathcal{I}_i \subseteq \mathcal{T}_\emptyset) = \prod_{t=n}^m p(\mathbf{m}_{\mathcal{T}_i}^t | \mathcal{I}_i \subseteq \mathcal{T}_\emptyset) = \prod_{t=n}^m \frac{1}{\alpha}, \quad (8)$$

Here, we compute frame-to-frame mask consistency as mask intersection-over-union between the mask prediction $\mathbf{m}^{(t-1) \rightarrow t}$ and the (mask) observation \mathbf{m}^t . The null hypothesis model is a confidence threshold (base value α), obtained by hyperparameter optimization.

Finally, the tube objectness score utilizes the objectness scores estimated by the network and integrates them over the whole tube:

$$\vartheta_{\text{obj}}(\mathcal{T}_i^{n:m}) = \ln \frac{p(s_{\mathcal{T}_i}^{n:m} | \mathcal{I}_i \subseteq \mathcal{T}_i^{n:m})}{p(s_{\mathcal{T}_i}^{n:m} | \mathcal{I}_i \subseteq \mathcal{T}_\emptyset)}, \quad (9)$$

$$\begin{aligned} p(s_{\mathcal{T}_i}^{n:m} | \mathcal{I}_i \subseteq \mathcal{T}_i^{n:m}) &= \prod_{t=n}^m p(s_{\mathcal{T}_i}^t | \mathcal{I}_i \subseteq \mathcal{T}_i^{n:t}) \\ &= \prod_{t=n}^m s^t, \end{aligned} \quad (10)$$

$$p(s_{\mathcal{T}_i}^{n:m} | \mathcal{I}_i \subseteq \mathcal{T}_\emptyset) = \prod_{t=n}^m p(s_{\mathcal{T}_i}^t | \mathcal{I}_i \subseteq \mathcal{T}_\emptyset) = \prod_{t=n}^m \frac{1}{\beta}. \quad (11)$$

Here the likelihood ratio test compares the probability of the tube being a valid objects (individual probabilities are estimated by the MP R-CNN network) against a null hypothesis model of the tube belonging to the segmentation clutter. The confidence threshold β is a model parameter.

Experimentally, we can observe (Sec. 3) that for *known* object categories, objectness scores extracted from a pre-trained variant of Mask R-CNN [11] provide a great ranking cue. However, for objects that were not in the training set, scores based on temporal mask and motion consistency lead to a significantly better ranking and provide better generalization for objects categories that were not seen during the training, *i.e.* that are not in the COCO category set. This observation confirms that all three terms of (2) are necessary.

Proposal Tubes Co-Selection. The image-level object proposals, obtained from the MP R-CNN network provide an over-segmentation of the image with several overlapping region proposals. Consequentially, the tube enumeration algorithm will produce several conflicting video tubes, that overlap in space-time. Intuitively, video tubes that closely overlap in space-time hypothesize the same object. In order to obtain a very compact video tube set, we perform an additional video tube co-selection step that discourages co-selection of tubes with a significant space-time overlap. The co-selection is performed by computing a MAP estimate using a CRF model by minimizing the following non-submodular function within batches of 100 frames:

$$F(\mathbf{b}, \mathcal{A}^{n:m}) = \sum_{\mathcal{T}_i \in \mathcal{A}^{n:m}} b_i (\epsilon_1 - \theta(\mathcal{T}_i)) + \epsilon_2 \cdot \sum_{\mathcal{T}_i, \mathcal{T}_j \in \mathcal{A}^{n:m}} b_i b_j \varphi(\mathcal{T}_i, \mathcal{T}_j) \quad (12)$$

$\mathbf{b} \in [0, 1]^{|\mathcal{A}^{n:m}|}$ is a binary vector whose elements b_i indicate that the i^{th} tube is selected. The unary term

$\theta(\cdot)$ corresponds to the tube scoring function. The pairwise term $\varphi(\mathcal{T}_i, \mathcal{T}_j) = \sum_{t=n}^m \ln(\text{IoU}(\mathbf{m}_i^t, \mathbf{m}_j^t))$ integrates image-level temporal mask IoU within the batch and gives a penalty to overlapping tubes. Here, \mathbf{m}_i^t and \mathbf{m}_j^t are object masks of tubes \mathcal{T}_i and \mathcal{T}_j at frame t , respectively. The model parameters ϵ_1 and ϵ_2 are learned on a held-out validation set of the KITTI dataset [7] using random search. Thus, co-selection of two video tubes with a significant temporal mask overlap is discouraged.

The presented Co-Selection reduces the set of video-object tube proposals, such that starting from the unlabelled images of a video sequence, we end up with a compact set of 4D Video Tubes for *known* and *unknown* object categories. Using this formulation, co-selection of tubes in which one represents an object and a second one a part of the same object is still possible. For our application, this is desired, because it is not trivial to separate objects and their parts in general. To minimize the energy function (12), we use the multi-branch algorithm by [49].

3. Experimental Evaluation

3.1. Datasets

We evaluate the proposed method on three datasets: COCO [28], Oxford RobotCar [30] and KITTI [7]. The KITTI dataset is a standard object detection and tracking benchmark in automotive scenarios, captured from a mobile platform equipped with a stereo camera setup. On KITTI, only a small subset of observed object classes is labeled, namely *car*, *pedestrian*, *truck*, *van*, and *cyclist*. In addition, a small set of object classes containing the categories *car trailer*, *motorcycle*, and *child strollers* is labeled as *misc*. We use the KITTI Multi-Object Tracking benchmark with the *car* and *pedestrian* categories for a sequence-level evaluation of the tracking accuracy of our 4D-GVT approach.

The Oxford RobotCar dataset was recorded from a car and covers a wide range of different seasons and lighting conditions. The dataset provides a large amount of recorded data (roughly 30 h) and covers a broad set of objects. However, there are no object class labels available. For evaluation purposes, we labeled a subset of the video sequences (see Tab. 1) in order to measure the performance of our method on *known* and *unknown* object classes.

3.2. Image-Level Proposal Evaluation

Evaluation on COCO. On the COCO [28] dataset, we follow the standard evaluation protocol and evaluate the performance of our model with the average recall (AR) metric for a fixed number of proposals using the minival split. We show that our proposed method achieves a high AR with only a few proposals per frame and that it is capable of generalizing to *unknown* object categories, *i.e.* categories that were held-out during the model training. We

Category	#instances	Portion
Car	599	40.1%
Person	354	23.1%
Bike	78	5.2%
Bus	50	3.3%
Other	413	27.6%
All	1494	100%

Table 1: We labeled a subset of the Oxford RobotCar dataset for evaluation purpose. We annotated objects of 5 categories on 150 images belonging to different video sequences.

follow the generalization experiment of Deepmask [41] and train the model using a subset of 20 categories that intersect with Pascal VOC [6]. We evaluate the generalization of our model against Deepmask [41], as the follow-up Sharpmask paper [42] does not provide generalization experiments. We report the numbers obtained by the authors from [41].

Table 2 outlines results obtained by training our (MP R-CNN20) model and the baseline (Deepmask20) on a 20-category subset and evaluating on the full COCO 80 category validation set. Our model performs and generalizes better than the DeepMask baseline. In particular, we achieve 0.261 AR (+0.122) compared to the baseline for top-10 box proposals. Remarkably, our model also performs better than the DeepMask20* variant (0.152 AR), which uses the fully-trained model for ranking the proposals. Our full model (MP R-CNN80) achieves 0.421 AR (+0.16 AR from the 20-category model). Table 3 highlights the difference between AR obtained on the *known* 20-category set and the full *unknown* 60-category set. As expected, the total recall (AR @ 1000) is lower for the *unknown* category set and we observe a loss in ranking capability. However, MP R-CNN is capable of proposing and segmenting object categories that do not appear in the training set and hence, is suitable for our purpose.

Evaluation on Oxford. To demonstrate the cross-domain transfer capabilities of MP R-CNN, we labeled a small subset of the Oxford Robotcar dataset (see the summary in Tab. 1). Using this set, we compare MP R-CNN to several baselines. All methods were trained on the COCO dataset, except Mask^X R-CNN [17], which was trained on both COCO and Visual Genome [21] with 3000 object categories. Fig. 3 shows recall (at > 0.5 IoU) as a function of the number of frame-level object proposals for *known* object categories (intersecting with COCO category set, *left*) and *unknown* object classes, (*right*). We compare our method (—) to Sharpmask [42] (Deepmask successor, —), Mask^X R-CNN (—) and two variants of Mask R-CNN. “M R-CNN original” (—) refers to a standard Mask R-CNN, where we merely keep the predictions that are assigned to the *background* class. “M R-CNN agnostic” (—) refers to a Mask R-CNN, trained in only a category agnostic setting, as explained in Sec. 2.1. Finally, (—) refers to a MP R-CNN after

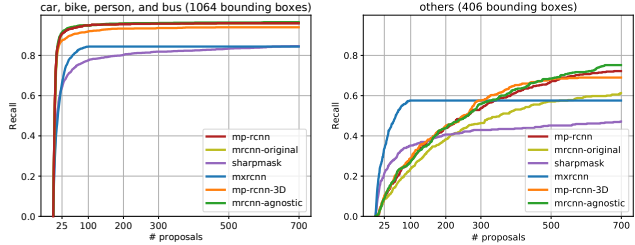


Figure 3: Per-frame object proposal recall evaluation (Oxford).

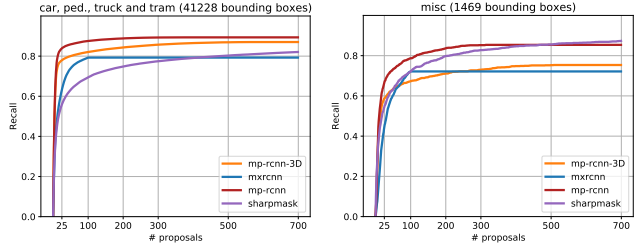


Figure 4: Per-frame object proposal recall evaluation (KITTI).

localizing objects in 3D space, as explained in Sec. 2.2.

As evident from Fig. 3 (left), our model (—) and other Mask R-CNN variants (—, —) perform well on *known* object categories while Sharpmask (—) and Mask^X R-CNN (—) achieve lower recall. On *unknown* object categories, Sharpmask (0.13 recall) and especially Mask^X R-CNN (0.21 recall) perform significantly better for top-10 proposals per frame and in general provide a better ranking. We attribute superior ranking capability of Mask^X R-CNN to the fact that it was trained on a large dataset, containing 3000 object classes. However, in a limit for 700 proposals per frame, MP R-CNN (—) and other Mask R-CNN variants (—, —) achieve higher recall (0.75) than Mask^X R-CNN (—) (0.59). In addition, the experiment (—) shows that not all objects can be robustly localized in 3D space due to limited depth estimation range and failures in depth estimation due to extreme weather or lighting conditions. Further experiments demonstrating similar trends on *known* object classes of the KITTI dataset and the additional *misc* category set (containing classes such as *car trailer*, *motorcycle* and *child strollers*) are shown in Fig. 9.

3.3. Video Tubes Evaluation

In this section, we demonstrate that the proposed 4D-GVT method performs well as a sequence-level object proposal method while being able to produce tubes that cover *unknown* arbitrary objects. We demonstrate sequence-level performance by evaluating our method on our custom split of the training set* from the KITTI Multi-Object Tracking dataset (KITTI MOT) [7].

*We used sequences 1,2,3,4,9,11,12,15,17,19,20 to perform model validation and the rest for the evaluation.

For the KITTI MOT evaluation we follow the official evaluation protocol that evaluates tracking performance using CLEAR-MOT [2] metrics on *car* and *pedestrian* categories, as only these categories are observed frequently enough so that tracking evaluation is statistically meaningful. In general, we do not know the object categories of the tubes. However, we can use the information obtained from the second (category-specific) classification head (as explained in Sec. 2.1) and obtain the probability for a tube representing a *car* or *pedestrian*. We compare our method to the tracking-by-detection approach by [37] (CIWT), which is among the top-4 performers on the KITTI MOT benchmark (comparing methods using public detections, Regionlets [60]) and which thus provides a strong object tracking baseline. This method is tuned for tracking *car* and *pedestrian* categories only. In addition, we compare to a stereo-based category-agnostic tracker (CAMOT) [38], that is capable of tracking a large variety of objects. To make the comparison fair, we use the same inputs from MP R-CNN, which is trained on COCO, for CAMOT and our method. In this case, we map COCO category *person* to *pedestrian*. As an additional experiment, we fine-tune MP R-CNN on the KITTI dataset on *car* and *pedestrian* categories, which we can use to evaluate CIWT. Note, that we output bounding boxes, derived from the tracked segments, whereas KITTI MOT assumes amodal bounding boxes.

Table 10 outlines the tracking results for the *car* and *pedestrian* categories, respectively. As can be seen, CIWT achieves the highest MOTA score (0.65) on the *car* category when fine-tuned on KITTI, and our 4D-GVT takes the second place (0.61). We attribute the performance loss on the *car* category to the fact that our method can only propose tubes in the camera-near range (up to 40m), whereas CIWT can also track in farther ranges in the absence of stereo. As expected, the fine-tuned methods perform better. For the *pedestrian* category, our method and CIWT both achieve 0.33 MOTA. These experiments demonstrate that our video-object proposal generator performs better than a state-of-the-art category-agnostic tracker and can compete with top-performing tracking-by-detection methods for *known* object categories. However, due to the tube co-selection over batches of 100 frames, our method is not online.

In order to demonstrate the generality of our proposed method, we evaluate 4D-GVT on the Oxford RobotCar dataset using the same evaluation protocol as for evaluating per-frame object proposals 3.2. We extract video tubes in a 100-frame temporal neighborhood of the 150 labeled images and evaluate recall on a video-frame level. We summarize the results in Fig. 5. We show the results obtained using the full tube set (—) and using the tubes obtained after the co-selection step (—), as explained in Sec. 2.2 for *known* objects (Fig. 5, left) and *unknown* objects (Fig. 5, right).

We evaluate our proposals against Mask^X R-CNN (—)

Model	Box Proposals			Segmentation Proposal		
	AR @ 10	AR @ 100	AR @ 1000	AR @ 10	AR @ 100	AR @ 1000
DeepMask20	0.139	0.286	0.431	0.109	0.215	0.314
DeepMask20*	0.152	0.306	0.432	0.123	0.233	0.314
MP R-CNN20	0.261	0.412	0.517	0.223	0.321	0.390
MP R-CNN80	0.421	0.608	0.662	0.355	0.494	0.539

Table 2: Following the evaluation protocol of DeepMask [41], we show the generalization capabilities of our proposal generator on image-level by training on 20 COCO categories and evaluating on all 80 COCO categories.

Evaluation Criteria	Box Proposals			Segmentation Proposals		
	AR @ 10	AR @ 100	AR @ 1000	AR @ 10	AR @ 100	AR @ 1000
Known COCO Categories (20)	0.421	0.587	0.641	0.348	0.468	0.511
Unknown COCO Categories (60)	0.069	0.179	0.338	0.053	0.134	0.241

Table 3: We evaluate our per-frame proposal generator on *known* and *unknown* categories separately. The trend indicates that the generator is able to generalize to unseen object categories given a sufficient number of proposals, while it performs reasonably on seen object categories. Remark: Since the ground-truth is different (*known* and *unknown*), the numbers are not directly comparable, but the trend is clear.

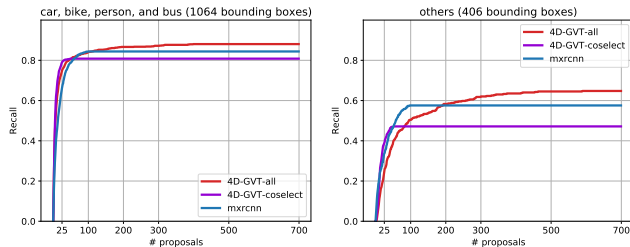


Figure 5: 4D-GVT recall evaluation (Oxford).

[17], which was trained jointly on COCO dataset (80 categories) using mask supervision and Visual Genome dataset [21] using bounding box supervision on 3000 categories. Here in case of *known* categories, we achieve higher recall with both 4D-GVT variants (—, —) in the top-10 proposals regime. For *unknown* categories, both Mask^X R-CNN (—) and 4D-GVT after co-selection (—) provide an excellent ranking for top-10 proposals. Mask^X R-CNN saturates at 0.58 recall, while 4D-GVT-all co-select saturates at 0.47 and 4D-GVT-all reaches a high recall at 0.64. Remarkably, our 4D-GVT proposals achieve this recall, despite being trained only on the 80 COCO categories, whereas Mask^X R-CNN requires an additional 3000-category training set.

These experiments demonstrate that by leveraging parallax as consistency filter, motion cues and object instance segmentation we can compensate for the absence of training data for *unknown* object categories. Fig. 7 compares the output of (a) our method, (b) Mask^X R-CNN and (c) Mask R-CNN qualitatively. To obtain Mask^X R-CNN results, we used the out-of-the-box implementation and visualization scripts provided by the authors; for Mask R-CNN we used the implementation by [61].

Finally, we experimentally justify the design decisions for tube scoring (Oxford) in Fig. 6. Clearly, for *known* object categories, tube ranking based on the integrated pro-

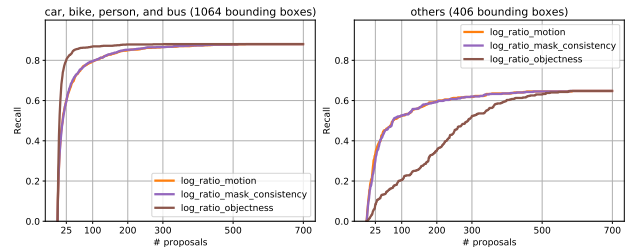


Figure 6: Tube scoring evaluation (Oxford).

posal confidence scores (**objectness**) obtained by MP R-CNN is a strong cue (Fig. 6, *left*). However, for *unknown* categories (Fig. 6, *right*), as already demonstrated by experiments performed on the COCO dataset, scores obtained by the network do not provide a reliable ranking cue. In this case, the scoring based on the **mask consistency score** and the **motion consistency score** provide significantly stronger scoring cues.

4. Conclusion

In this work we proposed 4D generic video-object tubes. We showed that it is indeed possible to detect and track objects from *known* and *unknown* categories as required by a wide range of robotics and automotive applications. We believe that this work is a starting point and there is still an enormous potential for further exploiting such data.

Acknowledgments: This project was funded, in parts, by ERC Consolidator Grant DeeVise (ERC-2017-COG-773161). The experiments were performed with computing resources granted by RWTH Aachen University under project rwth0275.

References

- [1] A. Bansal, K. Sikka, G. Sharma, R. Chellappa, and A. Divakaran. Zero-shot object detection. In *ECCV*, 2018. 1, 3

	MOTA	MOTP	IDS	Recall	Precision
CIWT (KITTI)	0.33	0.71	42	0.69	0.67
4D-GVT (KITTI)	0.33	0.68	18	0.59	0.70
CAMOT (KITTI)	0.26	0.68	72	0.63	0.65
4D-GVT (COCO)	0.27	0.71	24	0.71	0.62
CAMOT (COCO)	-0.05	0.71	214	0.74	0.51

	MOTA	MOTP	IDS	Recall	Precision
CIWT (KITTI)	0.65	0.79	8	0.82	0.84
4D-GVT (KITTI)	0.61	0.81	6	0.73	0.88
CAMOT (KITTI)	0.60	0.81	40	0.73	0.88
4D-GVT (COCO)	0.57	0.82	4	0.70	0.86
CAMOT (COCO)	0.54	0.81	174	0.74	0.84

Table 4: CLEAR-MOT evaluation on KITTI MOT dataset for the *pedestrian* (*left*) and *car* (*right*) category.

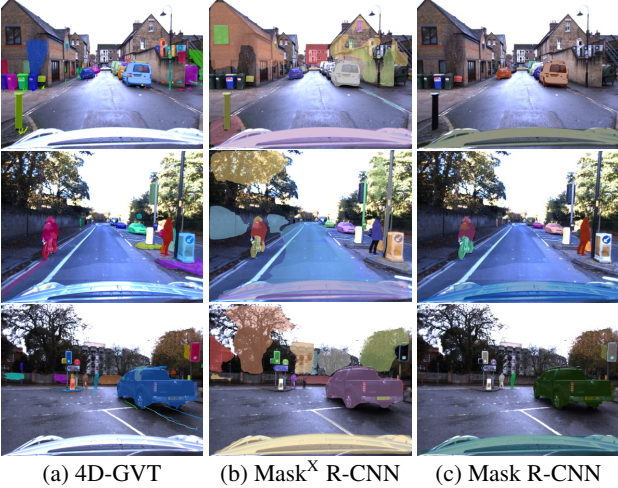


Figure 7: Qualitative comparison of proposed 4D-GVT to Mask R-CNN [11] and Mask^X R-CNN [17].

[2] K. Bernardin and R. Stiefelhagen. Evaluating multiple object tracking performance: The clear mot metrics. *JVIP*, 2008;1:1–1:10, 2008. [7](#), [11](#), [12](#)

[3] W. Brendel and S. Todorovic. Video object segmentation by tracking regions. In *ICCV*, 2009. [1](#), [2](#)

[4] J. Deng, W. Dong, R. Socher, L.-J. Li, K. Li, and L. Fei-Fei. ImageNet: A large-scale hierarchical image database. In *CVPR*, 2009. [11](#)

[5] A. Dewan, T. Caselitz, G. D. Tipaldi, and W. Burgard. Motion-based detection and tracking in 3d lidar scans. In *ICRA*, 2015. [2](#)

[6] M. Everingham, L. Van Gool, C. Williams, J. Winn, and A. Zisserman. The pascal visual object classes (VOC) challenge. *IJCV*, 88(2):303–338, 2010. [6](#)

[7] A. Geiger, P. Lenz, and R. Urtasun. Are we ready for autonomous driving? the KITTI vision benchmark suite. In *CVPR*, 2012. [2](#), [6](#), [7](#)

[8] A. Geiger, M. Roser, and R. Urtasun. Efficient large-scale stereo matching. In *ACCV*, 2010. [3](#), [4](#)

[9] A. Geiger, J. Ziegler, and C. Stiller. Stereoscan: Dense 3D reconstruction in real-time. In *Intel. Vehicles Symp.*, 2011. [4](#)

[10] R. Hartley and A. Zisserman. *Multiple view geometry in computer vision*. Cambridge University Press, 2000. [11](#)

[11] K. He, G. Gkioxari, P. Dollár, and R. Girshick. Mask R-CNN. In *ICCV*, 2017. [1](#), [2](#), [3](#), [5](#), [9](#), [11](#), [12](#), [16](#)

[12] K. He, X. Zhang, S. Ren, and J. Sun. Deep residual learning for image recognition. In *CVPR*, 2016. [11](#)

[13] D. Held, D. Guillory, B. Rebsamen, S. Thrun, and S. Savarese. A probabilistic framework for real-time 3d seg-mentation using spatial, temporal, and semantic cues. In *RSS*, 2016. [2](#)

[14] D. Held, J. Levinson, S. Thrun, and S. Savarese. Combining 3d shape, color, and motion for robust anytime tracking. In *RSS*, 2014. [2](#)

[15] E. Horbert, G. M. Garcia, S. Frintrop, and B. Leibe. Sequence-level object candidates based on saliency for generic object recognition on mobile systems. In *ICRA*, 2015. [2](#)

[16] R. Hou, C. Chen, and M. Shah. Tube convolutional neural network (t-cnn) for action detection in videos. In *ICCV*, 2017. [1](#)

[17] R. Hu, P. Dollár, K. He, T. Darrell, and R. Girshick. Learning to Segment Every Thing. In *CVPR*, 2018. [1](#), [2](#), [6](#), [8](#), [9](#), [12](#)

[18] Y. Hu, J. Huang, and A. Schwing. Maskrnn: Instance level video object segmentation. In *NIPS*, 2017. [1](#), [2](#)

[19] J. Huang, V. Rathod, C. Sun, M. Zhu, A. Korattikara, A. Fathi, I. Fischer, Z. Wojna, Y. Song, S. Guadarrama, and K. Murphy. Speed/accuracy trade-offs for modern convolutional object detectors. In *CVPR*, 2017. [16](#)

[20] S. Jin, A. RoyChowdhury, H. Jiang, A. Singh, A. Prasad, D. Chakraborty, and E. Learned-Miller. Unsupervised hard example mining from videos for improved object detection. In *European Conference on Computer Vision (ECCV)*, 2018. [2](#)

[21] R. Krishna, Y. Zhu, O. Groth, J. Johnson, K. Hata, J. Kravitz, S. Chen, Y. Kalantidis, L.-J. Li, D. A. Shamma, M. Bernstein, and L. Fei-Fei. Visual genome: Connecting language and vision using crowdsourced dense image annotations. *arXiv preprint arXiv:1602.07332*, 2016. [6](#), [8](#)

[22] S. Kwak, M. Cho, I. Laptev, J. Ponce, and C. Schmid. Unsupervised object discovery and tracking in video collections. In *ICCV*, 2015. [1](#), [2](#), [3](#)

[23] Y. J. Lee and K. Grauman. Object-graphs for context-aware visual category discovery. In *CVPR*, 2010. [1](#), [3](#)

[24] Y. J. Lee and K. Grauman. Learning the easy things first: Self-paced visual category discovery. In *CVPR*, 2011. [1](#), [3](#)

[25] B. Leibe, K. Schindler, N. Cornelis, and L. V. Gool. Coupled object detection and tracking from static cameras and moving vehicles. *PAMI*, 30(10):1683–1698, 2008. [2](#), [3](#), [4](#)

[26] P. Lenz, J. Ziegler, A. Geiger, and M. Roser. Sparse scene flow segmentation for moving object detection in urban environments. In *Intel. Vehicles Symp.*, 2011. [2](#)

[27] S. Li, B. Seybold, A. Vorobyov, A. Fathi, Q. Huang, and C.-C. J. Kuo. Instance embedding transfer to unsupervised video object segmentation. In *CVPR*, 2018. [1](#), [2](#)

[28] T.-Y. Lin, M. Maire, S. Belongie, J. Hays, P. Perona, D. Ramanan, P. Dollár, and C. L. Zitnick. Microsoft COCO: Common objects in context. In *ECCV*, 2014. [3](#), [6](#), [11](#)

[29] J. Luiten, P. Voigtlaender, and B. Leibe. Premvos: Proposal-generation, refinement and merging for video object segmentation. In *Asian Conference on Computer Vision*, 2018. 1

[30] W. Maddern, G. Pascoe, C. Linegar, and P. Newman. 1 year, 1000km: The Oxford RobotCar dataset. *IJRR*, 36(1):3–15, 2017. 1, 6, 12

[31] I. Misra, A. Shrivastava, and M. Hebert. Watch and learn: Semi-supervised learning of object detectors from videos. In *CVPR*, 2015. 2

[32] I. Misra, C. L. Zitnick, and M. Hebert. Shuffle and Learn: Unsupervised learning using temporal order verification. In *ECCV*, 2016. 2

[33] D. Mitzel and B. Leibe. Taking mobile multi-object tracking to the next level: People, unknown objects, and carried items. In *ECCV*, 2012. 2

[34] F. Moosmann and M. Sauerland. Unsupervised discovery of object classes in 3d outdoor scenarios. In *ICCV Workshops*, 2011. 2

[35] G. Neuhold, T. Ollmann, S. R. Bulo, and P. Kontschieder. The Mapillary Vistas dataset for semantic understanding of street scenes. In *ICCV*, 2017. 11

[36] A. Ošep, A. Hermans, F. Engelmann, D. Klostermann, M. Mathias, and B. Leibe. Multi-scale object candidates for generic object tracking in street scenes. In *ICRA*, 2016. 1, 2

[37] A. Ošep, W. Mehner, M. Mathias, and B. Leibe. Combined image- and world-space tracking in traffic scenes. In *ICRA*, 2017. 7

[38] A. Ošep, W. Mehner, P. Voigtlaender, and B. Leibe. Track, then decide: Category-agnostic vision-based multi-object tracking. *ICRA*, 2018. 1, 2, 4, 7

[39] D. P. Papadopoulos, J. R. R. Uijlings, F. Keller, and V. Ferrari. Extreme clicking for efficient object annotation. In *ICCV*, 2017. 11

[40] T. Pham, V. B. G. Kumar, T.-T. Do, G. Carneiro, and I. Reid. Bayesian semantic instance segmentation in open set world. In *ECCV*, September 2018. 2

[41] P. Pinheiro, R. Collobert, and P. Dollr. Learning to segment object candidates. In *NIPS*, 2015. 6, 8

[42] P. Pinheiro, T. Lin, R. Collobert, and P. Dollár. Learning to refine object segments. In *ECCV*, 2016. 6, 12

[43] A. Prest, C. Leistner, J. Civera, C. Schmid, and V. Ferrari. Learning object class detectors from weakly annotated video. In *CVPR*, 2012. 1, 3

[44] S. Rahman, S. H. Khan, and F. Porikli. Zero-shot object detection: Learning to simultaneously recognize and localize novel concepts. *arXiv preprint arXiv:1803.06049*, 2018. 1, 3

[45] D. B. Reid. An algorithm for tracking multiple targets. *IEEE Trans. Automatic Control*, 24(6):843–854, 1979. 2, 3, 4, 5

[46] M. Rubinstein, A. Joulin, J. Kopf, and C. Liu. Unsupervised joint object discovery and segmentation in internet images. In *CVPR*, 2013. 1, 3

[47] M. Rünz and L. Agapito. Co-fusion: Real-time segmentation, tracking and fusion of multiple objects. In *ICRA*, May 2017. 2

[48] B. C. Russell, W. T. Freeman, A. A. Efros, J. Sivic, and A. Zisserman. Using multiple segmentations to discover objects and their extent in image collections. In *CVPR*, 2006. 1, 3

[49] K. Schindler, J. U., and H. Wang. Perspective N-view multibody structure-and-motion through model selection. In *ECCV*, 2006. 6

[50] J. Sivic, B. C. Russell, A. Zisserman, W. T. Freeman, and A. A. Efros. Unsupervised discovery of visual object class hierarchies. In *CVPR*, 2008. 1, 3

[51] K. Tang, V. Ramanathan, L. Fei-fei, and D. Koller. Shifting weights: Adapting object detectors from image to video. In *NIPS*, 2012. 2

[52] A. Teichman, J. Levinson, and S. Thrun. Towards 3D object recognition via classification of arbitrary object tracks. In *ICRA*, 2011. 2

[53] A. Teichman and S. Thrun. Tracking-based semi-supervised learning. *IJRR*, 31(7):804–818, 2012. 2

[54] P. Tokmakov, C. Schmid, and K. Alahari. Learning to segment moving objects. *arXiv preprint arXiv:1704.05737*, 2017. 2

[55] Y.-H. Tsai, G. Zhong, and M.-H. Yang. Semantic co-segmentation in videos. In *ECCV*, 2016. 1, 3

[56] T. Tuytelaars, C. H. Lampert, M. B. Blaschko, and W. Buntine. Unsupervised object discovery: A comparison. *IJCV*, 88:284–302, 2010. 1, 3

[57] P. Voigtlaender and B. Leibe. Online adaptation of convolutional neural networks for video object segmentation. In *BMVC*, 2017. 1, 2

[58] C. Vondrick, A. Shrivastava, A. Fathi, S. Guadarrama, and K. Murphy. Tracking emerges by colorizing videos. In *ECCV*, September 2018. 1, 2

[59] L. Wang, G. Hua, R. Sukthankar, J. Xue, Z. Niu, and N. Zheng. Video object discovery and co-segmentation with extremely weak supervision. *PAMI*, 39:2074–2088, 2014. 1, 3

[60] X. Wang, M. Yang, S. Zhu, and Y. Lin. Regionlets for generic object detection. In *ICCV*, 2013. 7

[61] Y. Wu et al. Tensorpack. <https://github.com/tensorpack/>, 2016. 8, 11

[62] Y. Xian, C. H. Lampert, B. Schiele, and Z. Akata. Zero-shot learning - a comprehensive evaluation of the good, the bad and the ugly. *PAMI*, 2018. 1, 3

[63] L. Zhang, L. Yuan, and R. Nevatia. Global data association for multi-object tracking using network flows. In *CVPR*, 2008. 2

[64] G. Zhu, F. Porikli, and H. Li. Model-free multiple object tracking with shared proposals. In *ACCV*, 2016. 2

[65] J.-Y. Zhu, J. Wu, Y. Wei, E. Chang, and Z. Tu. Unsupervised object class discovery via saliency-guided multiple class learning. In *CVPR*, 2012. 1, 3

Supplemental Material

A. Implementation Details

A.1. MP R-CNN

MP R-CNN is based on a modified version of a Mask R-CNN [11] network implementation by [61] with a ResNet101 [12] backbone. We adjust this network to be category agnostic by replacing the N classes with just one class by mapping all classes to a single foreground class for detecting generic objects. Next, we add an additional classification head to the network, so that the network can recover the classification information for each object. We train this network starting from pre-trained ImageNet [4] weights on the COCO dataset [28]. The batch size is one image per GPU that is resized (without changing the aspect ratio) such that the smaller image dimension is 800, if the resulting larger image dimension is no more than 1333. Otherwise, it is resized such that the larger image dimension is 1333 pixels. For optimization, we use the Momentum Optimizer of Tensorflow with an initial learning rate of $3 * 10^{-3}$, a momentum of 0.9 and a learning rate decay schedule as given by [61]. We train this network for 854,100 steps using four TITAN X Pascal GPUs. For data augmentation, we adopt horizontal flipping. Furthermore, we perform non-maximum suppression to remove proposals which have an IoU of 80% or greater with a higher scoring proposal. However, we do not threshold by the score.

A.2. 4D-GVT

Ground Plane Estimation. For video-tubes estimation, we utilize coarse geometric scene knowledge by estimating a ground plane. To perform the ground plane estimation, we i) use the knowledge about the camera height in order to trim-down the point-cloud, ii) estimate the ground plane with the RANSAC algorithm and iii) refine the estimate of the RANSAC inliers using linear least squares.

Kalman Filter. We leverage linear constant-velocity to estimate the 3D position and size of the video tube. In addition, we use a Kalman filter for the 3D segment-to-tube association and tube scoring. Based on the 3D localization of the per-frame object proposals in a 3D point cloud, we can robustly compute a median 3D position estimate of the segment and an estimate of the 3D bounding box as explained in the paper. Our approach uses the x and z coordinates directly and obtains the observed y -coordinate estimate by projecting the estimated 3D median position to the ground. Thus, we obtain a projection of the 3D position to the estimated ground plane. This has proven to be very robust to partial occlusions. Similarly, we project the 3D velocity estimate to the ground. In the case that the 3D velocity of a segment was not estimated reliably (e.g. the object is

not well-textured to obtain feature matches), we update the state using only partial observations of the state (3D position and the 3D size estimates). Assuming constant pixel and disparity noise, we obtain the uncertainty in 3D localization and velocity as the uncertainty estimate of the stereo depth estimate using forward error propagation [10].

Hyperparameter Learning. All hyperparameters for tube generation, scoring, and co-selection are learned on the KITTI dataset using *car* and *pedestrian* categories, optimized for the MOTA score [2]. In particular, we use sequences 1, 2, 3, 4, 9, 11, 12, 15, 17, 19 and 20 to perform model validation and the rest for the evaluation. For the video-object mining, we manually lower the CRF model parameter ϵ_1 in order to allow tubes representing *unknown* object categories to be selected as well and assign equal weights (0.33) to w_1, w_2 and w_3 , *i.e.*, to all three terms that contribute to the tube score. Hyperparameter learning would assign a significantly higher weight to the objectness term (weight w_3) since in KITTI only *known* objects are evaluated, *i.e.*, the *car* and *pedestrian* categories.

A.3. KITTI Fine-tuning of Mask R-CNN

In order to evaluate a KITTI fine-tuned version of Mask R-CNN (the results marked with (KITTI) in Table 4 of the main paper), we use the detections of TrackR-CNN. TrackR-CNN extends Mask R-CNN by 3D convolutions in order to incorporate temporal context. It is pre-trained on COCO [28] and Mapillary [35] and fine-tuned on novel pixel-wise annotations for the KITTI tracking training set.

B. Additional Experimental Evaluation

B.1. Oxford RobotCar Labels

In this section, we provide additional details on the Oxford RobotCar labels, which we only used for the recall evaluation. We did not use these labels for training or tuned any hyperparameters using these labels. For the labeling process, we manually selected 150 images which are not too close to each other in time. We labeled 1,494 (1,081 *known*, 413 *unknown*) bounding boxes covering the visible portions of objects (non-amodal) by clicking the extremal points [39]. Examples of labeled objects are shown in Fig. 8. Labeled categories that overlap with the COCO [28] category set are *car*, *person*, *bike* and *bus*. In addition, we labeled several object classes that are not present in the COCO dataset as “other” (pink color). Most notable object classes in the *unknown* set are the following: *signage*, *pole*, *stone road sign*, *traffic cone*, *street sign*, *rubbish bin*, *transformer*, *post box*, *booth*, *stroller*.



Figure 8: Examples of labeled images from Oxford RobotCar [30] dataset. The *unknown* object classes are assigned label “other” (pink color).

B.2. Image-Level Proposal and Video Tubes Evaluation

Due to lack of space, we omitted a detailed presentation of the recall evaluation in the main paper. Additional KITTI per-frame proposal evaluation results are shown in Fig. 9, Table 7 (car and pedestrian) and 8 (unknown classes). For the latter, we further separate the *misc* class and combinations of *misc* and classes, which are only remotely related to those in COCO, *i.e.*, *pedestrian - cyclist, car - van*.

Tables 5 and 6 present a detailed recall evaluation for per-frame object proposals and video tubes (4D-GVT), respectively. Specifically, we present the precise recall we obtain for the top-10, 25, 50, 100 and 150 per-frame proposals and video tubes. As in the main paper, **mrcnn-original** refers to vanilla Mask R-CNN [11], **mrcnn-agnostic** refers to a Mask R-CNN variant trained in the category-agnostic setting, **sharpmask** refers to [42], **mxrcnn** refers to Mask^X R-CNN [17] and finally, **mp-rcnn** and **mp-rcnn-3D** refer to our proposed MP R-CNN, and MP R-CNN with 3D localization, respectively.

In the main paper, we excluded from the CLEAR-MOT tables the less commonly used Mostly-Tracked (MT), Mostly-Lost (ML) and Fragments metrics [2]. For completeness, we show all tracking metrics evaluated on the KITTI benchmark in Tables 9 (car) and 10 (pedestrian).

B.3. Video-Mining Evaluation

Table 11 shows statistics of the tracks we obtained by mining 14h of the Oxford RobotCar dataset. In total, we obtained 977,622 tracks, of which 833,293 are of an *unknown* class. This number is significantly larger than the number of tracks for the most common classes such as *person* and *car*. 501 tracks are classified as COCO categories which are very unlikely to occur in the RobotCar dataset (*e.g. elephant*) and most likely stem from classification er-

rors. The average length of our tracks is 18.3 time frames.

B.4. Additional Qualitative Results

Fig. 11 shows additional qualitative results (a) of our method, (b) Mask R-CNN [11], (c) and (d) of Mask^X R-CNN [17] with and without score-based thresholding on the Oxford RobotCar dataset. We use the original threshold as provided by [17]. In Fig. 10, we compare qualitative results produced by our MP R-CNN on image-level with the final proposals obtained from 4D-GVT. The examples show that our method is capable of producing a compact set of object proposals on videos.

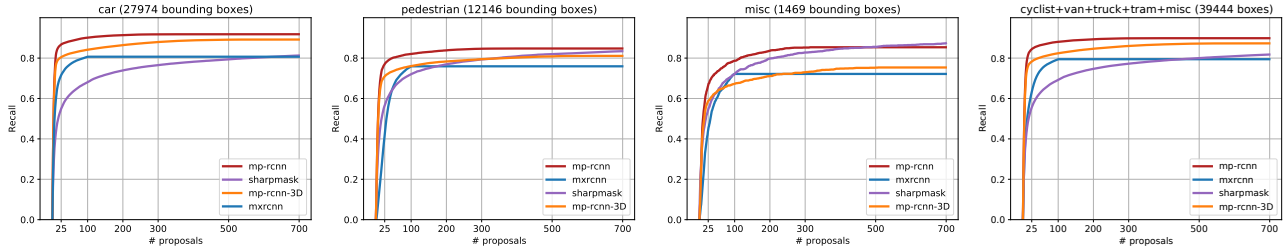


Figure 9: Recall of different strategies for obtaining object proposals as a function of the number of object proposals per frame (KITTI). This is an extended version of the Fig. 4 in the main paper.

	10	25	50	100	700
mrcnn-agnostic	0.81	0.91	0.94	0.95	0.97
mrcnn-original	0.78	0.91	0.94	0.95	0.96
mp-rcnn	0.81	0.91	0.93	0.95	0.96
mp-rcnn-3D	0.79	0.87	0.90	0.92	0.94
mxrcnn	0.44	0.66	0.79	0.84	0.84
sharpmask	0.49	0.64	0.72	0.78	0.85

	10	25	50	100	700
mrcnn-agnostic	0.02	0.09	0.17	0.27	0.75
mrcnn-original	0.02	0.08	0.14	0.24	0.61
mp-rcnn	0.01	0.09	0.16	0.28	0.72
mp-rcnn-3D	0.02	0.10	0.18	0.29	0.69
mxrcnn	0.21	0.34	0.47	0.58	0.58
sharpmask	0.13	0.21	0.28	0.35	0.47

Table 5: Recall of different strategies for obtaining object proposals as a function of number of object proposals per-frame (Oxford RobotCar, left: *known*, right: *unknown*).

	10	25	50	100	700
4D-GVT-all	0.59	0.75	0.81	0.84	0.88
4D-GVT-coselect	0.66	0.79	0.81	0.81	0.81
mxrcnn	0.44	0.66	0.79	0.84	0.84

	10	25	50	100	700
4D-GVT-all	0.10	0.25	0.39	0.50	0.65
4D-GVT-coselect	0.17	0.39	0.47	0.47	0.47
mxrcnn	0.21	0.34	0.47	0.58	0.58

Table 6: Recall for the proposed 4D-GVT, compared to Mask^X R-CNN as a function of the number of object proposals per frame (Oxford RobotCar, left: *known*, right: *unknown*).

	10	25	50	100	700
mp-rcnn	0.82	0.87	0.88	0.90	0.92
mp-rcnn-3D	0.77	0.80	0.82	0.84	0.89
sharpmask	0.43	0.55	0.62	0.68	0.81

	10	25	50	100	700
mp-rcnn	0.65	0.77	0.80	0.82	0.85
mp-rcnn-3D	0.61	0.71	0.74	0.76	0.81
sharpmask	0.42	0.57	0.65	0.72	0.83

Table 7: Recall of different strategies for obtaining object proposals as a function of the number of object proposals per frame (KITTI, *known* classes; left: *car*, right: *pedestrian*).

	10	25	50	100	700
mp-rcnn	0.50	0.67	0.73	0.79	0.85
mp-rcnn-3D	0.45	0.59	0.63	0.67	0.75
sharpmask	0.41	0.54	0.63	0.72	0.87

	10	25	50	100	700
mp-rcnn	0.77	0.84	0.86	0.88	0.90
mp-rcnn-3D	0.73	0.78	0.80	0.82	0.87
sharpmask	0.43	0.56	0.63	0.69	0.82

Table 8: Recall of different strategies for obtaining object proposals as a function of number of object proposals per-frame (KITTI, *unknown* classes; left *misc*, right: *cyclist, van, truck, tram, misc*).

	MOTA	MOTP	MT	ML	IDS	Recall	Fragments	Precision
CIWT (KITTI)	0.33	0.71	0.54	0.10	42	0.69	123	0.67
4D-GVT (KITTI)	0.33	0.68	0.34	0.15	18	0.59	157	0.70
CAMOT (KITTI)	0.26	0.68	0.34	0.09	72	0.63	224	0.65
4D-GVT (COCO)	0.27	0.71	0.53	0.10	24	0.71	138	0.62
CAMOT (COCO)	-0.05	0.71	0.57	0.03	214	0.74	321	0.51

Table 9: CLEAR-MOT evaluation on KITTI MOT dataset for *car* category. This is an extended version of Tab. 4 in the main paper.

	MOTA	MOTP	MT	ML	IDS	Recall	Fragments	Precision
CIWT (KITTI)	0.65	0.79	0.62	0.05	8	0.82	82	0.84
4D-GVT (KITTI)	0.61	0.81	0.53	0.14	6	0.73	46	0.88
CAMOT (KITTI)	0.60	0.81	0.52	0.09	40	0.73	92	0.88
4D-GVT (COCO)	0.57	0.82	0.51	0.20	4	0.70	34	0.86
CAMOT (COCO)	0.54	0.81	0.51	0.09	174	0.74	237	0.84

Table 10: CLEAR-MOT evaluation on KITTI MOT dataset for *pedestrian* category. This is an extended version of Tab. 4 in the main paper.

Category	#Tracks	Avg. Track Length (Frames)	Median Track Length (Frames)
<i>person</i>	59,605	24.0	12.0
<i>car</i>	49,227	33.1	13.0
<i>bicycle</i>	17,324	21.7	12.0
<i>traffic light</i>	5,802	60.1	17.0
<i>truck</i>	2,255	44.8	24.0
<i>motorcycle</i>	2,063	24.8	12.0
<i>handbag</i>	2,013	14.1	8.0
<i>bus</i>	1,591	46.2	17.0
<i>bench</i>	867	23.3	12.0
<i>backpack</i>	813	16.8	5.0
<i>potted plant</i>	666	28.6	17.0
<i>umbrella</i>	565	17.5	11.0
<i>stop sign</i>	269	51.6	25.0
<i>chair</i>	263	20.3	11.0
<i>suitcase</i>	160	22.6	15.5
<i>fire hydrant</i>	147	22.4	9.0
<i>parking meter</i>	99	31.1	10.0
<i>train</i>	70	15.5	8.0
<i>dog</i>	27	20.2	10.0
<i>cat</i>	2	6.0	6.0
<i>unknown</i>	833,293	16.5	8.0
<i>other COCO</i>	501	20.5	11.0
Total	977,622	18.3	9.0

Table 11: Statistics for mining 14h of Oxford data. Other COCO are categories which are unlikely to occur in outdoor street scenes (probably classification errors).



(a) Frame proposals (Mask Proposal R-CNN)



(b) Video Tube Proposals (4D-GVT)

Figure 10: Qualitative comparison between (a) proposals on frame level obtained from MP R-CNN and (b) proposals on video-level generated by our 4D-GVT method.

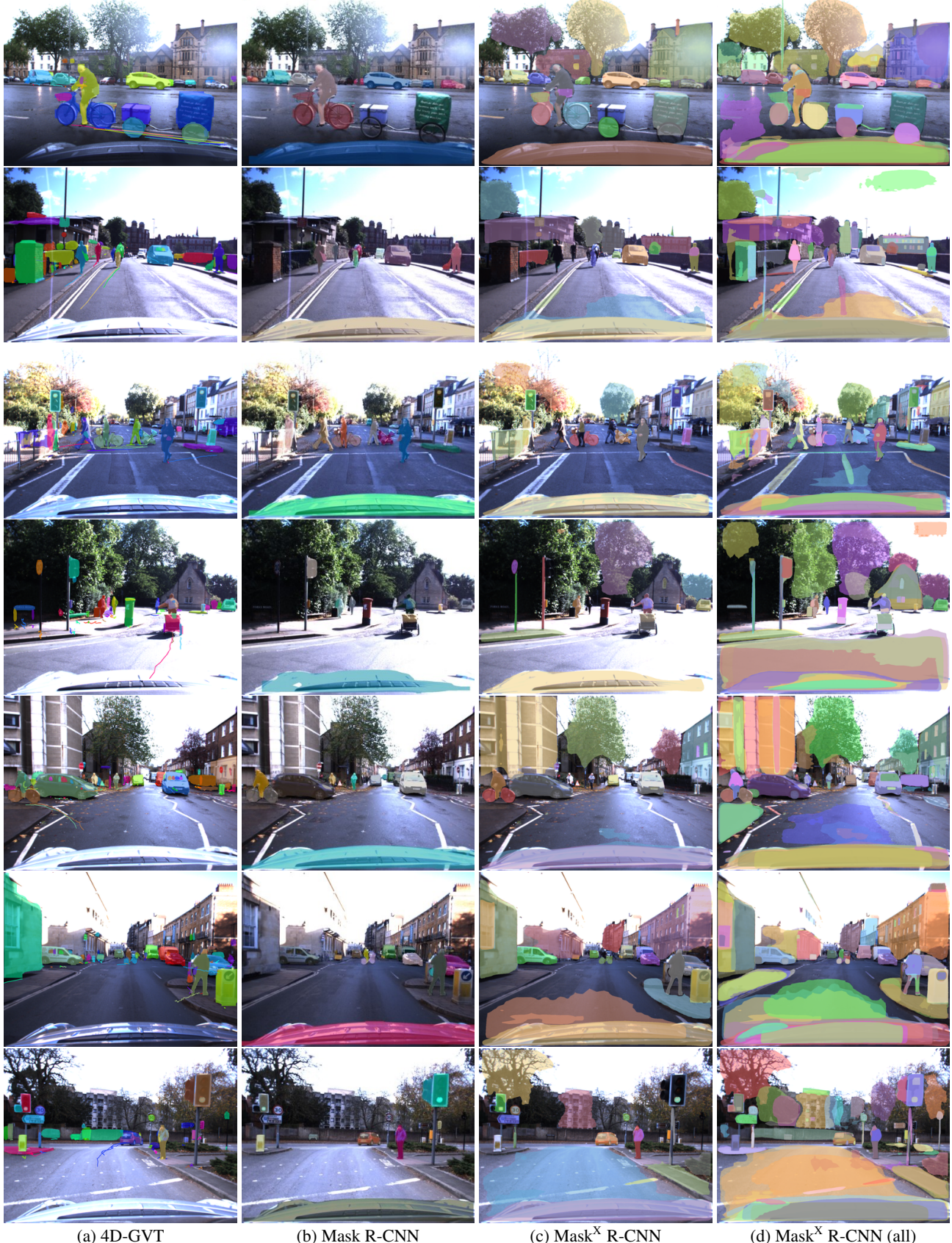


Figure 11: Qualitative comparsion of our proposed (a) 4D-GVT, (b) Mask R-CNN [11], (c) Mask^X R-CNN [19]; (d) additionally visualizes all Mask^X R-CNN instance segmentations (non-thresholded using the recommended settings) on the Oxford RobotCar dataset. As can be seen, our approach generates a better interpretation for the relevant street scene objects, while producing fewer clutter proposals overall.